engineering proceedings

MDPI

Proceeding Paper

Stress and Strain Analysis of Ocular Resonant Frequencies with Different Axial Lengths †

Jiehui Zheng [1,2], Peng-San Cheng [3], Chia-Wen Lee [1,2], Chao-Ming Hsu [3,*], Linda Yi-Chieh Poon [4,5] and Cheng-Fu Yang [6,7,*]

[1] Marine Culture & Tourism Integration of Fujian Higher Educational Applied Liberal Arts Research Center, Xiamen 361102, China; zhengjiehui@xmoc.edu.cn (J.Z.); lijiawen@xmoc.edu.cn (C.-W.L.)
[2] School of Information Engineering, Xiamen Ocean Vocational College, Xiamen 361102, China
[3] Department of Mechanical Engineering, National Kaohsiung University of Science and Technology, Kaohsiung 807, Taiwan; f110142127@nkust.edu.tw
[4] Department of Ophthalmology, Kaohsiung Chang Gung Memorial Hospital, Kaohsiung 833, Taiwan; lindap@cgmh.org.tw
[5] School of Medicine, Chang Gung University, Taoyuan 333, Taiwan
[6] Department of Chemical and Materials Engineering, National University of Kaohsiung, Kaohsiung 811, Taiwan
[7] Department of Aeronautical Engineering, Chaoyang University of Technology, Taichung 413, Taiwan
* Correspondence: jammy@nkust.edu.tw (C.-M.H.); cfyang@nuk.edu.tw (C.-F.Y.)
† Presented at the 9th Eurasian Conference on Educational Innovation 2026 (ECEI 2026), Da Nang City, Vietnam, 30 January–2 February 2026.

Abstract

Using the finite element analysis software ANSYS (version 2020), we investigated the variation trends in the resonant frequencies of the eyeball, as well as the stress and strain distributions in the optic nerve under different intraocular pressures. To better understand the mechanical and physical characteristics of the eyeball, the reliability and accuracy of ophthalmic research were enhanced. A total of six 3D eyeball models were constructed using SolidWorks (version 2023), including one porcine eyeball model and five human eyeball models with axial lengths of 22, 24, 26, 28, and 30 mm. These axial lengths correspond respectively to hyperopia, emmetropia, and myopia of approximately −6.00, −12.00, and −18.00 diopter, representing different refractive states of the human eye. The models were imported into ANSYS, where the Harmonic Response and Modal Analysis modules were applied to determine the resonant and natural frequencies, and to analyze their trends with respect to axial length variation. The simulation results revealed that, in the modal analysis, the natural frequency decreased with increasing axial length, indicating that longer eyes (more myopic) are more susceptible to lower-frequency vibrations. Despite the frequency differences, the mode shapes under identical modal orders remained highly similar across all models, demonstrating consistent vibrational behavior among eyes of different axial lengths. These findings contribute valuable biomechanical insights into the vibrational characteristics of the eyeball and provide theoretical support for future ophthalmological and biomedical engineering applications, including ocular diagnostics and protective device design.

Keywords: element analysis software; ANSYS; intraocular pressures (IOP); hyperopia; emmetropia

Check for updates

Academic Editors: Teen-Hang Meen and Chun-Yen Chang

Published: 5 June 2026

Copyright: © 2026 by the authors. Licensee MDPI, Basel, Switzerland. This article is an open access article distributed under the terms and conditions of the Creative Commons Attribution (CC BY) license.

1. Introduction

The human eye is a complex biomechanical organ whose optical and mechanical stability are essential for maintaining normal vision. The interplay between intraocular pressure (IOP), ocular tissue elasticity, and geometrical configuration governs both visual performance and the structural integrity of the eye. Abnormal mechanical conditions, such as elevated IOP or elongated axial length, have been strongly associated with vision-threatening disorders, including glaucoma and high myopia. The World Health Organization has identified glaucoma as a major global cause of irreversible blindness, emphasizing the urgent need to understand the mechanical mechanisms underlying optic nerve damage [1].

Although elevated IOP is the primary biomechanical risk factor for glaucoma, it does not independently determine disease onset. Instead, it acts as a mechanical loading condition that induces deformation and stress concentration within the optic nerve head and adjacent scleral tissues. When IOP exceeds the tissue's mechanical tolerance, chronic strain accumulation may lead to axonal disruption and progressive visual field loss. The equilibrium of IOP is maintained by the dynamic balance between aqueous humor production and outflow resistance through the trabecular meshwork.

With the rapid advancement of modern technology, the performance and computational capabilities of electronic devices have improved dramatically. This progress has, in turn, accelerated the development of numerical simulation software, which relies heavily on hardware performance and high-speed computing power. As a result, numerical simulation techniques have become increasingly prevalent across various engineering disciplines, providing researchers and engineers with efficient and accurate tools for analyzing complex physical phenomena. By integrating computer-aided design (CAD) and computer-aided engineering (CAE), it is now possible to construct detailed digital models and perform in-depth analyses to predict the mechanical, thermal, or fluid dynamic behavior of a system before physical prototyping [2,3].

CAD enables the creation of precise geometric models, while CAE facilitates performance evaluation and design optimization through simulation and computation. The combination of these technologies significantly reduces development time and cost, enhances design reliability, and enables iterative improvement of product performance. Numerical simulation has become an indispensable component of modern engineering research and product development, supporting the transition from traditional empirical approaches to data-driven engineering design.

In glaucomatous eyes, elevated IOP commonly results from increased hydrodynamic resistance rather than excessive aqueous humor secretion [4]. Understanding how IOP interacts with ocular geometry and tissue properties is therefore crucial for elucidating the pathophysiological development of glaucoma and other pressure-induced ocular diseases. Recently, finite element analysis (FEA) has become a powerful computational approach for investigating the biomechanical behavior of ocular structures. Through FEA, it is possible to simulate complex interactions among ocular components, analyze stress–strain distributions, and predict deformation patterns under various physiological and pathological conditions.

Studies have demonstrated that variations in axial length, a key geometric parameter differentiating hyperopic, emmetropic, and myopic eyes, can significantly affect both the vibrational characteristics and mechanical responses of the eyeball. Longer axial lengths, commonly associated with high myopia, are hypothesized to reduce the natural and resonant frequencies of the eyeball, making it more susceptible to external mechanical perturbations and structural instability.

https://doi.org/10.3390/engproc2026141007

On the basis of such concepts, we investigated the influence of axial length variation on the vibrational behavior and biomechanical response of the eyeball. Six 3D ocular models were constructed using SolidWorks (version 2023), including one porcine eyeball and five human eyeball models with axial lengths of 22, 24, 26, 28, and 30 mm, corresponding respectively to hyperopic, emmetropic, and myopic eyes. These models were analyzed using ANSYS (version 2020) finite element software under both modal and harmonic response analyses to determine the natural and resonant frequency variations as well as the stress and strain distributions in the optic nerve under different intraocular pressures.

Through systematic numerical simulation, the results of this study provide a basis to explain the relationship between ocular geometry and dynamic mechanical behavior. The results also contribute to an understanding of how axial elongation affects the resonant frequency, stress distribution, and structural stability of the eye. This research not only enhances the biomechanical comprehension of ocular function but also offers theoretical support for future applications in ophthalmic diagnostics, disease prevention, and the design of protective or corrective ocular devices.

2. Methodology

In this study, ANSYS Workbench 2020 R2 was employed for conducting FEA simulations. The analysis process was divided into pre-processing and post-processing. During the pre-processing stage, the appropriate analysis module was selected based on the simulation objectives. Material properties were then defined within the material library, where essential parameters such as elastic modulus, Poisson's ratio, and density were specified and assigned to the model components.

Subsequently, the model underwent geometric preparation and meshing, ensuring sufficient element density and quality to achieve accurate computational results while maintaining reasonable computational efficiency. Boundary conditions and external loads—such as IOP or other mechanical constraints—were applied to simulate realistic physiological conditions. These steps formed the foundation for the numerical analysis, enabling the accurate evaluation of stress distribution, strain response, and vibrational behavior of the eyeball structure under different design parameters.

Due to individual physiological differences, the dimensions of the human eyeball vary slightly among individuals. In this study, the geometric parameters of the ocular components were obtained from ophthalmological data and relevant literature sources [5,6]. The 3D models of the eyeball were constructed using the CAD software SolidWorks. The model developed in this study represents the left human eye, which consists of multiple anatomically distinct components, including the sclera, cornea, ciliary body, suspensory ligament (zonule fibers), optic nerve, aqueous humor, and vitreous body.

The entire eyeball is surrounded externally by a circular adipose layer, replicating the orbital fat that provides mechanical cushioning and structural stability. The geometric configuration and dimensions of each part are illustrated in Figure 1. All adjacent components were precisely aligned and connected, ensuring a seamless interface between anatomical regions without any gaps or overlaps to preserve physiological realism.

In both the modal analysis and harmonic response analysis, the simulation conditions were established with reference to the experimental setup of Ref. [7]. First, the fixed boundary surface was constructed in the Design Modeler module, where the inner and outer diameters of the circular constraint area were defined as 6.3 and 8.3 mm, respectively, corresponding to the cylindrical fixation dimensions described in a previous study. This surface was subsequently constrained in the Static Structural module, where all axial displacements were set to zero. Additionally, a gravitational load of 9.8 m/s^2 was applied. Upon completion of the static structural analysis, the resulting stress–strain state was

https://doi.org/10.3390/engproc2026141007

imported into the Modal Analysis module to determine the natural frequencies of the system. For the harmonic response analysis, the obtained natural frequency data were used as input conditions, and intraocular pressure was applied to the interior surface of the eyeball model. Through this procedure, the resonance frequencies at the selected observation points on the sclera were obtained.

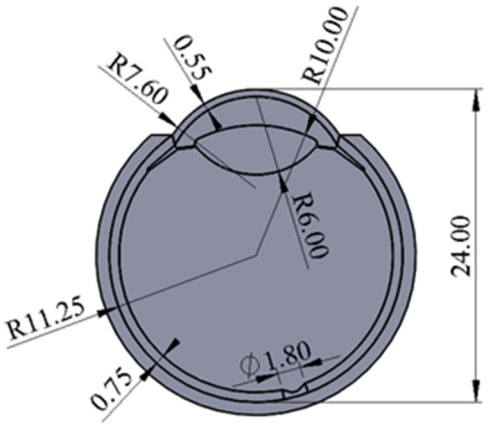


Figure 1. The geometric configuration and dimensions of each part of an eyeball.

The dimensions of the reference (normal) eye model were based on average anatomical measurements: an axial length of 24 mm, a maximum equatorial diameter of 22.5 mm, a corneal radius of 7.6 mm, a corneal thickness of 0.55 mm, a scleral radius of 11.25 mm, and a scleral thickness of 0.75 mm. The lens curvature radii were defined as 10 mm for the anterior surface and 6 mm for the posterior surface. The optic nerve was positioned slightly below and to the left of the central visual axis, with a maximum diameter of approximately 1.8 mm.

In total, six different eyeball models were constructed for comparative analysis: one porcine eye model, which served as an experimental validation reference, and five human eye models with varying axial lengths of 22, 24, 26, 28, and 30 mm. These human models respectively correspond to hyperopia (22 mm), emmetropia (24 mm), and myopia of −6.00 (26 mm), −12.00 (28 mm), and −18.00 diopters (30 mm). This systematic variation in axial length enables the investigation of the relationship between ocular geometry, resonant frequency, and biomechanical stress–strain behavior across different refractive conditions.

3. Results and Discussions

According to the experimental results reported in Ref. [7], the first resonance frequency was observed near approximately 24 Hz, at which point the measurement location exhibited a significant increase in vibration amplitude. The second resonance frequency was identified within the range of 90–100 Hz, where the measurement point similarly demonstrated a prominent oscillation behavior, as indicated by the red curve in Figure 2. In the present simulation, the first notable amplitude response occurred at 24 Hz, while the second resonance frequency was obtained at 98 Hz, as shown by the blue curve in Figure 2. A comparison between the simulation and experimental results shows that the simulated first resonance frequency matches the experimentally observed value. For the second resonance frequency, the simulated result differs from the reported value by approximately 6.5%; however, it remains within the 90–100 Hz range indicated in the reference study. Based on this consistency, the current structural model is deemed valid and is subsequently adopted for the continuation of this research.

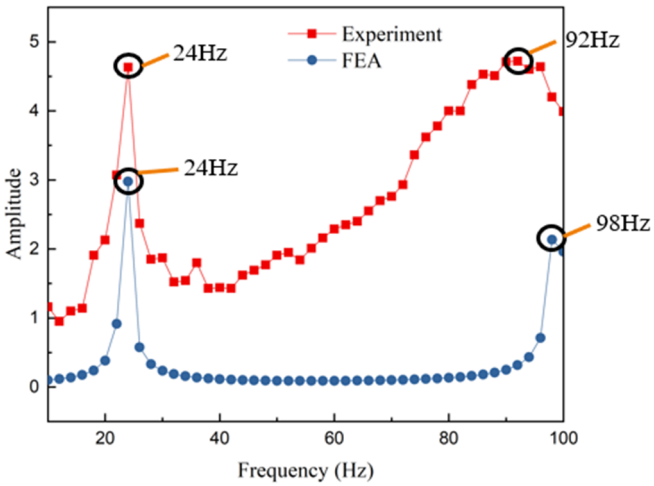


Figure 2. Comparison of the experimental and simulated results. Red line: experimental results; blue line: simulation results.

Subsequently, the natural frequencies and corresponding mode shapes of eyeballs with different axial lengths were analyzed. Figures 3–5 illustrate the first six natural frequencies and their associated vibration modes for axial lengths of 22 mm, 26 mm, and 30 mm, respectively (results for 24 mm and 28 mm are omitted here for brevity), while the overall comparison of all cases is summarized in Table 1.

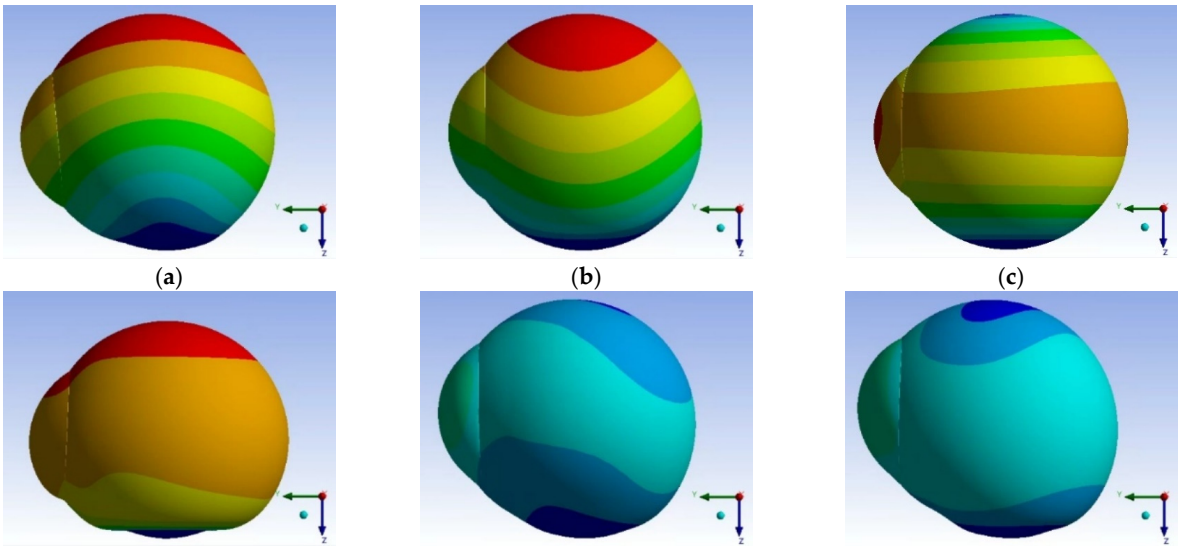


Figure 3. Six modal frequencies and mode shapes for the eyeball with a 22 mm axial length. (**a**) Model 1, (**b**) Model 2, (**c**) Model 3, (**d**) Model 4, (**e**) Model 5, and (**f**) Model 6.

Table 1. Comparisons of the six modal frequencies and mode shapes for eyeballs with different axial lengths.

Axial Length/Mode	Frequency (Hz)					
	1	**2**	**3**	**4**	**5**	**6**
22 mm	27.65	28.94	92.35	114.7	154.83	169.39
24 mm	25.79	26.02	86.38	105.99	157.98	164.74
26 mm	24.42	24.83	80.02	99.67	144.19	147.77
28 mm	22.38	23.08	73.51	92.76	133.49	149.07
30 mm	20.81	21.97	68.34	86.75	126.73	147.63

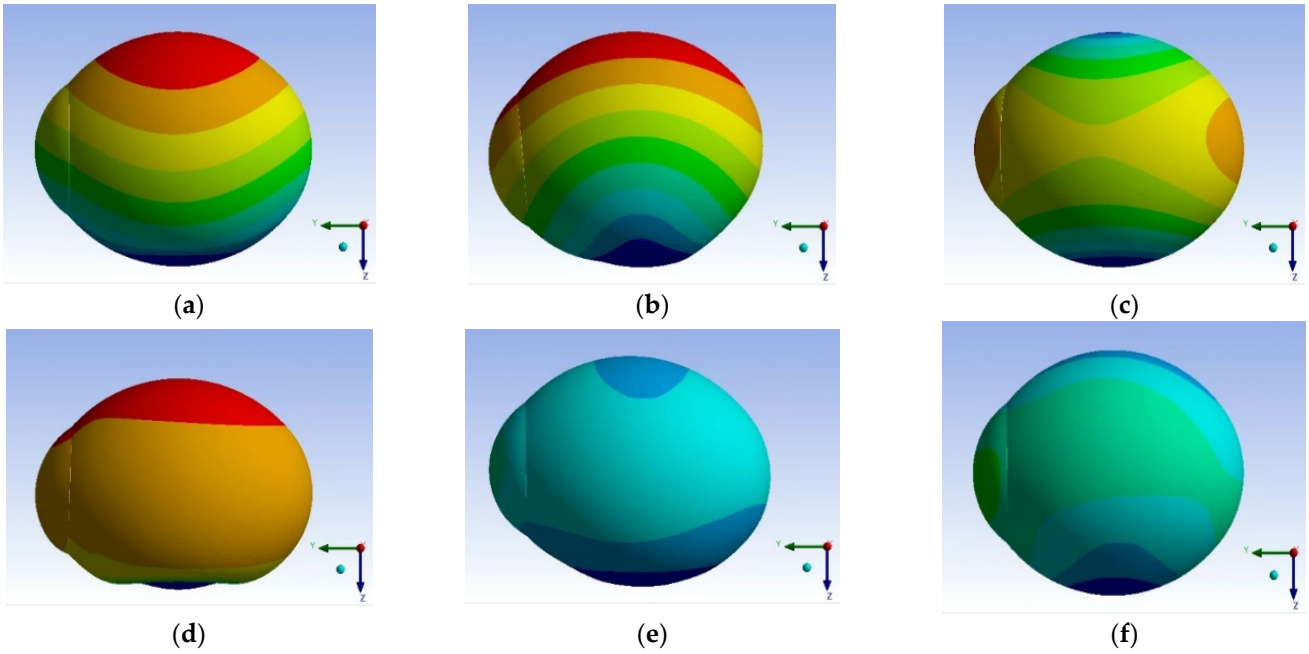


Figure 4. Six modal frequencies and mode shapes for the eyeball with a 26 mm axial length. (**a**) Model 1, (**b**) Model 2, (**c**) Model 3, (**d**) Model 4, (**e**) Model 5, and (**f**) Model 6.

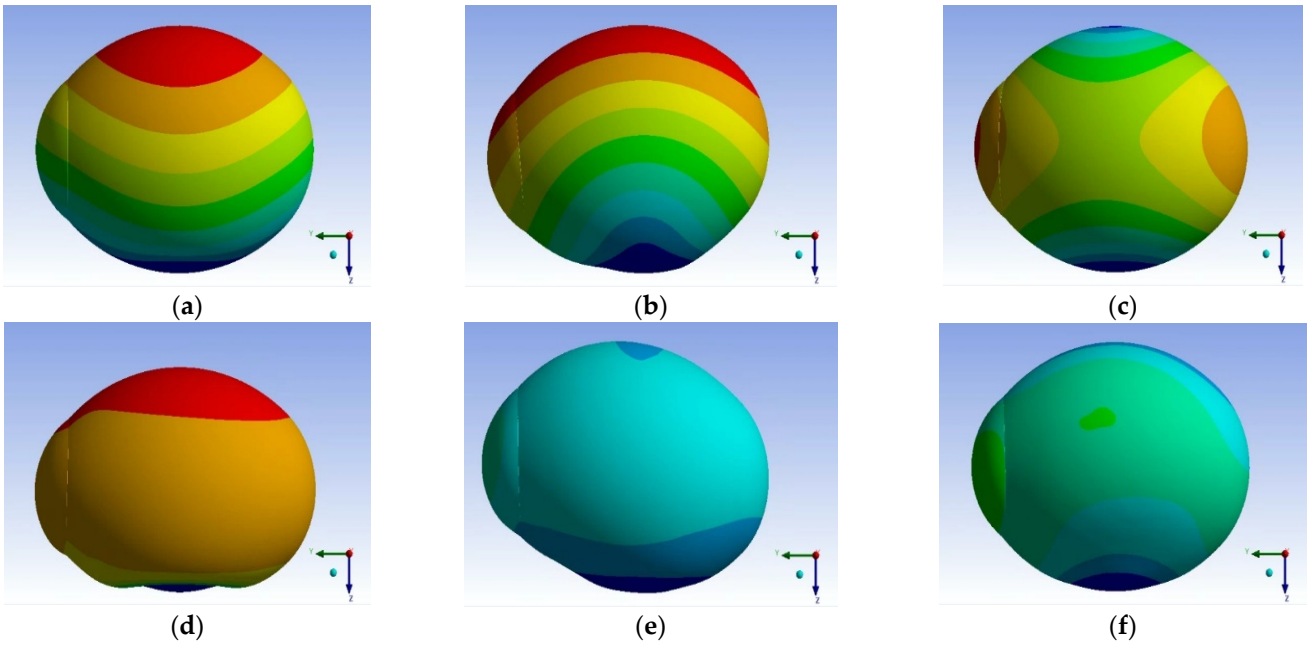


Figure 5. Six modal frequencies and mode shapes for the eyeball with a 30 mm axial length. (**a**) Model 1, (**b**) Model 2, (**c**) Model 3, (**d**) Model 4, (**e**) Model 5, and (**f**) Model 6.

The displacement directions of each mode shape can be clearly identified through the color contour variations. The color gradients indicate the distribution and intensity of vibration across the eyeball structure. The analysis results revealed that, for all five axial-length configurations, both the first and second mode shapes exhibit large displacement amplitudes primarily along the *Z*-axis, suggesting that these modes correspond to longitudinal or axial vibrations of the eyeball. In contrast, the third mode shape shows dominant displacement along the *Y*-axis, implying lateral oscillation behavior. The fourth mode shape again presents substantial *Z*-axis displacement, similar to the first and second modes, but with a noticeably greater vibration amplitude.

https://doi.org/10.3390/engproc2026141007

For the fifth and sixth modes, the overall displacement amplitude becomes relatively smaller, indicating that these higher-order modes contribute less to large-scale motion and are more localized in nature. The mode shape analysis indicates that the dynamic behavior of the eyeball is highly dependent on its geometric characteristics, particularly the axial length. Lower-order modes (first to fourth) are characterized by global oscillations that can significantly affect the deformation of the ocular shell. These modes are more likely to be excited by external mechanical disturbances or physiological pulsations, such as ocular micro-movements induced by heartbeat or intraocular pressure fluctuations.

As the axial length increases, a downward trend in the natural frequency values can be observed (Table 1), reflecting a reduction in overall structural stiffness. This shift implies that eyes with longer axial lengths—typical of myopic conditions—are more susceptible to resonance within lower-frequency ranges. Such frequency shifts may have clinical implications, as resonance within physiologically relevant frequency bands could lead to localized stress accumulation in the sclera or optic nerve head, potentially contributing to the development or progression of ocular disorders such as glaucoma or posterior staphyloma. Therefore, the correlation between axial length and modal characteristics provides valuable insights into the biomechanical stability of the eye, offering a foundation for future investigations into how mechanical resonance might influence ocular health and disease mechanisms.

Figure 6 illustrates the variation trends of the six natural frequencies for eyeballs with five different axial lengths. The first and second modal frequencies are relatively close for all axial lengths. Starting from the third mode up to the sixth mode, it can be observed that eyeballs with longer axial lengths exhibit lower natural frequencies compared to those with shorter axial lengths. Overall, the results indicate that the first mode is the most easily excited, with its corresponding frequency ranging from 20.81 to 27.65 Hz across the different axial lengths. From the perspective of mode shapes, the first through fourth modes show significant deformation amplitudes, suggesting that these modes contribute most to the global oscillation of the eyeball structure. In contrast, the fifth and sixth modes have comparatively smaller effects on the overall displacement of the model. The observed decrease in natural frequency with increasing axial length can be attributed to changes in structural stiffness and mass distribution.

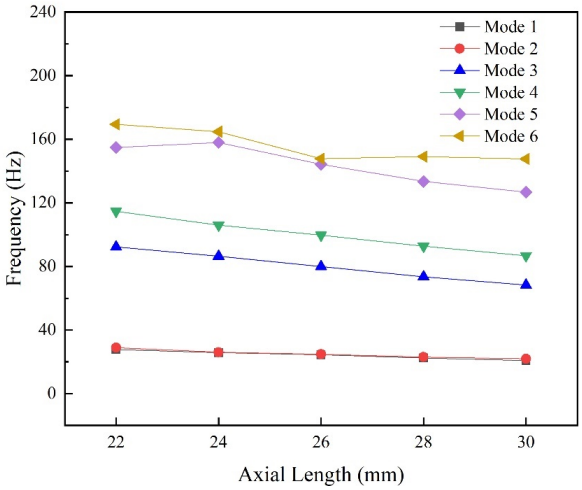


Figure 6. Analysis results of the six modal frequencies for five different axial lengths.

As the eyeball elongates, the effective radial stiffness of the sclera is reduced, resulting in a lower restoring force during deformation. Consequently, longer axial-length eyes, such as those associated with myopia, are dynamically more compliant and thus more

https://doi.org/10.3390/engproc2026141007

susceptible to resonance under external or physiological excitations. Clinically, this is a meaningful observation. If the natural frequencies of the eyeball fall closer to frequencies produced by physiological sources (e.g., ocular pulse pressure or extraocular muscle tremor), resonance-induced mechanical stress may more easily occur in elongated eyes.

The results can be applied to structural remodeling processes, such as scleral thinning, or to the analysis of increased stress concentrations at the optic nerve—factors that are relevant to the onset and progression of conditions including high myopia and glaucoma. Therefore, understanding the vibrational characteristics of eyes with different axial lengths is important not only from a biomechanical modeling perspective but also for guiding clinical evaluation and preventive strategies related to ocular health.

4. Conclusions

In this study, the dynamic characteristics of the eyeball were investigated through modal and harmonic response analyses under various axial length conditions. The simulation results showed strong agreement with previously reported experimental data, particularly for the first resonance frequency, with the second resonance frequency also falling within the experimentally observed range, demonstrating the validity and reliability of the established finite element model. The analysis results of the natural frequencies and mode shapes revealed that the first and second modes consistently exhibited dominant displacement along the *Z*-axis for all axial lengths, indicating that these modes are primarily associated with axial vibration of the eyeball. The third mode showed major displacement in the *Y*-axis direction, while the fourth mode returned to *Z*-axis-dominant deformation with higher amplitude.

The fifth and sixth modes demonstrated comparatively minor global displacement, suggesting that higher-order modes contribute less to the dynamic motion of the eye. The results indicated that as the axial length increases, the natural frequencies progressively decrease, particularly from the third to the sixth mode. This implies that elongated eyes, such as those commonly seen in high myopia, possess lower structural stiffness and therefore exhibit greater susceptibility to resonance under physiological or external mechanical excitation. The frequency range of the first mode (20.81–27.65 Hz) suggests that this mode is the most likely to be triggered under typical ocular or environmental vibration conditions. These findings highlight the importance of considering axial length when evaluating the biomechanical stability of the eyeball. The observed correlation between axial elongation and dynamic deformation response may contribute to understanding the progression of myopia-related scleral remodeling and the increased vulnerability of elongated eyes to mechanical stress. This study provides a foundation for future research aimed at exploring ocular tissue mechanics, pathological development, and potential clinical interventions for maintaining ocular structural integrity.

Author Contributions: Conceptualization, J.Z., P.-S.C., C.-W.L., C.-M.H., L.Y.-C.P. and C.-F.Y.; methodology, J.Z., P.-S.C., C.-W.L., C.-M.H., L.Y.-C.P. and C.-F.Y.; software J.Z., P.-S.C., C.-W.L., C.-M.H., L.Y.-C.P. and C.-F.Y.; validation, J.Z., P.-S.C., C.-W.L., C.-M.H., L.Y.-C.P. and C.-F.Y.; formal analysis, J.Z., P.-S.C., C.-M.H. and C.-F.Y.; investigation, C.-W.L., C.-M.H., L.Y.-C.P. and C.-F.Y.; data curation, J.Z., P.-S.C., C.-W.L., C.-M.H., L.Y.-C.P. and C.-F.Y.; writing—original draft preparation, J.Z., P.-S.C., C.-M.H. and C.-F.Y.; writing—review and editing, J.Z., P.-S.C., C.-M.H. and C.-F.Y.; visualization, J.Z., P.-S.C., C.-M.H. and C.-F.Y. All authors have read and agreed to the published version of the manuscript.

Funding: This research was funded by the Natural Science Foundation of Xiamen, China, grant No. 3502Z202573327, and the Marine Culture & Tourism Integration of Fujian Higher Educational Applied Liberal Arts Research Center, grant No. HYWL20240204.

Institutional Review Board Statement: Not applicable.

Informed Consent Statement: Not applicable.

Data Availability Statement: Data are contained within the article.

Conflicts of Interest: The authors declare no conflicts of interest.

References

1. Thylefors, B.; Negrej, A.D. The Global Impact of Glaucoma. *Bull. World Health Organ.* **1994**, *72*, 323–326. [PubMed]
2. Zheng, J.; Cheng, C.-C.; Hsu, C.-M.; Lee, C.-W.; Wu, P.-C.; Poon, L.Y.-C.; Yang, C.-F. Using Simulation Method to Analyze the Intraocular Pressure at Different Postures and Eye Movement Angles. *Sens. Mater.* **2025**, *35*, 2081–2090. [CrossRef]
3. Lee, C.-W.; Hsiao, H.-Y.; Hsu, C.-M.; Hsiao, C.-K.; Wang, Q.; Yang, C.-F. Analyses of How the Design of Hybrid Performance Stabilization System Affects Spinal Motion and Intervertebral Disc Pressure using Finite Element Method. *Sens. Mater.* **2025**, *35*, 2105–2114. [CrossRef]
4. Sigal, I.A.; Flanagan, J.G.; Ethier, C.R. Factors influencing optic nerve head biomechanics. *Investig. Ophthalmol. Vis. Sci.* **2005**, *46*, 4189–4199. [CrossRef] [PubMed]
5. Quigley, H.A.; Brown, A.E.; Morrison, J.D.; Drance, S.M. The Size and Shape of the Optic Disc in Normal Human Eyes. *Arch. Ophthalmol.* **1990**, *108*, 51–57. [CrossRef] [PubMed]
6. Sigal, I.A.; Grimm, J.; Schuman, J.S.; Kagemann, L.; Ishikawa, H.; Wollstein, G. A Method to Estimate Biomechanics and Mechanical Properties of Optic Nerve Head Tissues from Parameters Measurable Using Optical Coherence Tomography. *IEEE Trans. Med. Imaging* **2014**, *33*, 1381–1389. [CrossRef] [PubMed]
7. Shih, P.-J.; Guo, Y.-R. Resonance Frequency of Fluid-Filled and Prestressed Spherical Shell-A Model of the Human Eyeball. *J. Acoust. Soc. Am.* **2016**, *139*, 1784–1792. [CrossRef] [PubMed]

Disclaimer/Publisher's Note: The statements, opinions and data contained in all publications are solely those of the individual author(s) and contributor(s) and not of MDPI and/or the editor(s). MDPI and/or the editor(s) disclaim responsibility for any injury to people or property resulting from any ideas, methods, instructions or products referred to in the content.